Research Article Vol. 56, No. 36 / December 20 2017 / Applied Optics 9925

applied optics

Insight into aspheric misfit with hard tools: mapping the island of low mid-spatial frequencies

David Walker,[1,2,3,4] Wu Hsing-Yu,[2,3,*] Guoyu Yu,[1,3] Hongyu Li,[1,3,5] Wang Zhang,[2,5] and Chunlian Lu[2,6,1]

[1]University of Huddersfield, at the National Facility for Ultra Precision Surfaces, OpTIC-Centre, St Asaph, N. Wales, LL17 0JD, UK
[2]University College London, Department of Physics and Astronomy, Gower St, London, WC1E 6BT, UK
[3]National Facility for Ultra Precision Surfaces, OpTIC-Centre, St Asaph, N. Wales, LL17 0JD, UK
[4]Zeeko Ltd, Colville, Leicestershire, LE67 3WF, UK
[5]Research Center for Space Optical Engineering, Harbin Institute of Technology, Harbin 150001, China
[6]Key Laboratory in In-Fiber Integrated Optics, Ministry Education of China. College of Science, Harbin Engineering University, 15001 Harbin, China
*Corresponding author: andy810301@gmail.com

Received 18 July 2017; revised 1 November 2017; accepted 7 November 2017; posted 8 November 2017 (Doc. ID 297916); published 13 December 2017

This paper addresses computer numerical control (CNC) polishing of aspheric or freeform optics. Prior CNC grinding of the asphere tends to produce mid-spatial frequencies (MSFs) at some level. *Precessions* polishing can rectify these, but the very ability of the bonnet tooling to adapt to the local asphere enables it to do so, at least in part, to similar spatial frequencies in the MSFs. To accelerate smoothing, hard tools can, in principle, be used, but aspheric misfit is often assumed to preclude this. In this paper, we explore new insight into the role of abrasive particle size in accommodating misfit. First, we report on a glass-bending rig to produce a continuous range of complex surfaces, while withstanding process forces. Then, we describe how this was used to evaluate the triangle of misfit, abrasive size, and MSFs produced for hard rotating tools. This has revealed a regime in which such tools can be used without introducing significant new MSFs, as evidenced by manufacture of prototype off-axis aspheric segments for the European Extremely Large Telescope project.

OCIS codes: (220.0220) Optical design and fabrication; (220.1250) Aspherics; (220.4610) Optical fabrication; (240.5450) Polishing; (240.6700) Surfaces.
https://doi.org/10.1364/AO.56.009925

1. INTRODUCTION

As is well known, incorporating aspheric or freeform surfaces in an optical system can improve performance, using fewer optical surfaces, giving reduced system size and mass, or delivering functionality otherwise impossible. When computer numerical control (CNC) grinding the base asphere or freeform in a brittle material, or CNC polishing thereafter, the tool traditionally contacts the part over a small area. Otherwise, the misfit of tool and surface would lead to gross mid-spatial frequency (MSF) surface features. The small tool progresses over the surface along the defined tool path, with *position* being precisely controlled (grinding) [1], or *dwell time* (polishing) [2,3]. Even in ultraprecision grinding, MSFs arise from superposition of adjacent tool paths ("cusping"), positional errors, and dynamic effects. MSFs seen after polishing arise from various causes, including grinding print-through, misfit of polishing tools, the effects of overlapping tool paths, and the spatial frequencies inherent in the tool's influence function.

Considerable ingenuity has been directed to overcoming these issues. Various types of passive polishing tools embodying a compliant layer have been used to improve adaptation to the local asphere, but this compromises ability to remove input MSFs and may cause edge misfigure. The stressed lap [4] is hard, but actively deformed to match the local asphere, and so can polish and smooth aspheric surfaces within its dynamic range. However, it is a complex electromechanical system that, at some level, has to be re-built for each different job. Non-Newtonian tools can remove MSF from aspheres [5]. However, the natural frequency response of the material precludes the fast tool rotation often called upon for high-speed local corrective polishing.

These issues came to a head when polishing prototype 1.4 m off-axis aspheric mirror segments for the European Extremely Large Telescope (E-ELT), on the 1.6 m Zeeko CNC polishing machine at the OpTIC Center in North Wales. These prototypes were to the original 42 m aperture, 84 m ROC E-ELT

design. Unlike any other mirror segments made elsewhere for large telescopes, these were processed entirely in the final hexagonal shape, demanding precise control of edge profiles in polishing, as well as MSFs. Compliant, precessed-bonnet polishing was used, giving near-Gaussian influence functions. The tool-lift algorithm progressively decreased the spot size approaching the edges, in order to leave narrow turned-up edge features. A hard pitch tool was then used on the same machine, both to smooth the global surface and to suppress the edge upturns. The development of this method has previously been reported [6–9] and resulted in prototype segments that passed acceptance by the European Southern Observatory [10,11].

Controlling MSFs and/or edge misfigure confronts wider applications than just large telescope segments. This has prompted us to re-visit this most simple of smoothing methods—the use of a hard rigid tool. The question arises, "Why did this work on *off-axis aspheric* surfaces?" We posit that there must be a useful window, where the abrasive grit size is sufficient to accommodate the misfit "gaps." This paper explores this specific question experimentally, and is a development of work previously reported on what we term "grolishing" (intermediate processes between grinding and polishing) [12–15].

To this end, we have built a bending rig to deform a glass sheet, to create continuously variable aspheric surfaces, and also importantly, *to withstand process forces*. We report on using this to evaluate the quantitative relationships among misfit, abrasive size, and MSFs produced. Coarser abrasives than would be used for polishing were selected to give a large dynamic range and for experimental convenience. The results can be summarized in what we believe is a simple and general rule, which is reinforced by the segment polishing experience we outline later in this paper.

2. GLASS-BENDING RIG TO PRODUCE FREEFORMS

In order to investigate creation of MSFs, smooth input surfaces are needed. However, base curvature is not relevant, as the tool would be machined to match that of the part. For our experiments, a nominally flat tool working a freeform signature on a nominally flat part was satisfactory. We created the signature by deforming a commercially available 3 mm thick flat glass sheet (Fig. 1), previously cemented to a 2 mm thick aluminum alloy "bending plate." The deformation was applied by an adjustable screw pulling down on a metal pull-bar attached across the center of the plate. After processing the deformed part, it was returned to the unstressed, nominally flat state to facilitate surface measurements.

The dimensions of the bending rig were determined by availability of:

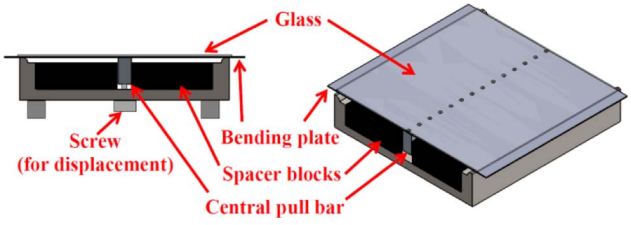

Fig. 1. Glass-bending rig.

i. A convenient and well-proven 100 mm brass diameter grolishing tool [12,13,15].

ii. Machine capacity—three robots; Zeeko IRP600 and 1200 CNC polishing machines [13].

iii. Measuring instrumentation—Talysurfs, Swinging Part Profilometer [16], 4D Technologies and Fisba interferometers, Pioneer DEA6 10.6 Coordinate Measuring Machine (CMM), and 180 mm diameter beam expander.

A. Process Flow for Using the Rig to Create Freeforms

The main purposes of the experimental procedures are set out in Figs. 2 and 3, summarized as sample preparation, tool conditioning, grolishing, post polishing, and measurement. After that, the sample returns to step 1 for subsequent experiments. The effects of grolishing raster spacing of 2, 5, 10, and 20 mm were evaluated by orthogonal post polishing. At 20 mm, a raster signature in the post-polished interferometer data became discernable, so 10 mm was selected for further use (i.e., a raster spacing of 10% of tool diameter is the maximum). Note that, after polishing in step 5 of Fig. 2, 10 s elapsed to relax the glass. Residual internal stresses were not considered further, because they tend to cause global deformations (which are removed in analysis), rather than MSFs.

B. Preparation of the Glass-Bending Rig

1. Adhesives to Attach the Glass to the Bending Plate

The adhesive for cementing the glass to the bending plate was required (i) to provide a strong bond to withstand bending stresses, (ii) to exhibit limited elasticity without cracking to

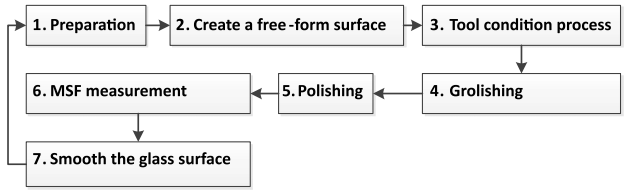

Fig. 2. Procedures for using the glass-bending rig.

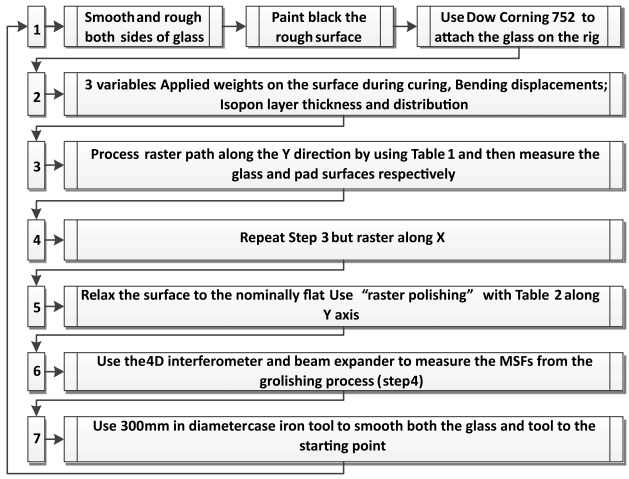

Fig. 3. More details of the 7 steps in Fig. 2.

enable the glass to return to nominally flat when bending stresses were removed, and (iii) to be easily removable, allowing detachment of the glass. Five adhesives were examined: (i) soft wax (35% paraffin wax +35% beeswax +30% resin), (ii) hard wax (25% paraffin wax +25% beeswax +50% resin), (iii) 7.36.20 Blanchard wax (from J. H. Young Company Ltd.), (iv) Power glue (UniBond 8081/1605193), and (v) Dow Corning 752 (silicone). The waxes were all too hard. Dow Corning 752 had an adequate combination of elasticity and hardness, and proved easier to remove than UniBond, so 752 silicone was selected. The thickness of the 752 silicone attaching the glass to the bending plate was 2 mm ± 0.05 mm. By using the Swinging Part Profilometer, the surface stability can be maintained with the processing load lower than 75 N.

2. Support and Filler Materials

A thin sheet of glass cemented to a thin metal bending plate will naturally deform under grolishing forces, which would disturb misfit. To circumvent this, the plate required a uniform, hard support underneath. Most of the void under the plate was occupied by solid spacer blocks, leaving a residual gap of 5 mm. This was filled with a polymeric filler that naturally molded itself to accommodate the stressed form of the bending plate. The filler needed to cure to a hard condition over a time sufficient for molding to complete, but not so long as to inconvenience experiments. The filler also needed to be chemically inert in the presence of slurry. Of various materials tested, Isopon (P38/1) car body filler proved best, curing in under 40 min to full hardness. Its tenacious adhesion required isolation, so that the rig could be easily reconfigured. Standard cling film was stretched over the spacer blocks, the filler applied with a comb, another layer of cling film applied, and the bending plate assembly lowered on top. The filler is inexpensive, widely available, and considered disposable when the rig is reconfigured for another bending regime.

Isopon was found to expand during curing, and this, combined with the addition of weights to the upper surface of the glass, was exploited in controlling glass surface form. For example, a near-cylindrical form (Fig. 4) could be obtained, or a saddle [Fig. 6(b)]. These represent two of the most useful surface forms for investigating the effects of tool misfit. A surface with a strong cylindrical term is the simplest to achieve. However, this surface is less suitable for investigating non-rotating tools following a tool path, as these tools will tend to wear into intimate contact. Rotating tools will wear only to the best rotationally averaged fit, and then exhibit cyclic misfit. The saddle form is more complex to set up, but applicable to rotating and non-rotating tools.

3. Mid-Spatial Frequency Measurement

Grolished surfaces, after the bending forces were relaxed, were of course not measurable using a visible interferometer. With a Talysurf Intrastylus profilometer, MSFs were masked by surface noise. Therefore, the relaxed, grolished surface was lightly prepolished on a Zeeko IRP1200 machine, using a raster tool path orthogonal to the grolishing tool path (in order to decouple effects of the two processes). A test plate was gently lowered into contact with the surface and illuminated under monochromatic 587.6 nm light (filtered mercury vapor lamp). Initially, using a test plate, double reflections between the glass surfaces

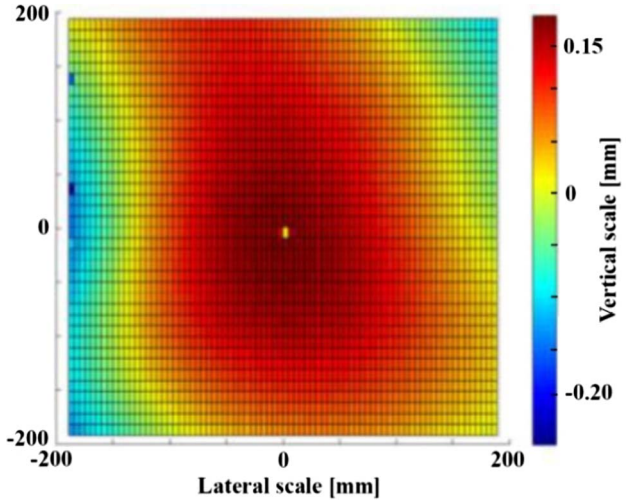

Fig. 4. Surface with a strong cylindrical term created by the expanding Isopon effect, as measured by the CMM.

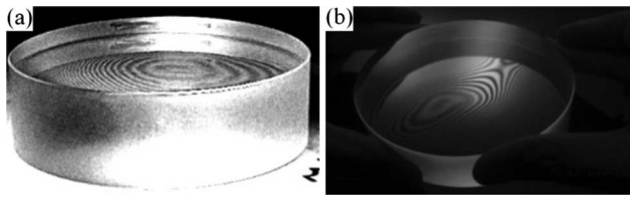

Fig. 5. Fringes from test plate (a) without matt black paint and (b) with matt black paint.

reduced fringe contrast. Therefore, the rear of the glass was roughened and painted matt black before applying adhesive. Fringes are shown in Fig. 5.

3. EXPERIMENTS

A. Create a Saddle Surface

The aim was to provide a range of representative forms to investigate tool misfit effects, rather than any specific form. As shown in Fig. 6, bending force, Isopon thickness, and applied weights enabled a peak-to-valley (PV) ~470 μm saddle-like surface to be produced. The resulting saddle-like surfaces were used to characterize MSFs arising from different misfits with a rotating rigid tool.

Figure 7 shows the glass-bending rig on (a) the robot grolishing station and (b) the Zeeko IRP1200 polishing machine, both at OpTIC. Process parameters are shown in Tables 1 and 2, as per [11,12,17].

B. Measurement of Results

1. Surface of the Hard-Pad Grolishing Tool

The tool was first conditioned with 30 μm Al_2O_3 abrasive on the deformed glass on the bending rig. Note that the central hole in the pad, which allowed abrasive slurry to be injected on-axis [Fig. 8(a)], avoided slurry being immediately expelled centrifugally, as when using peripheral delivery. Because the pad was rotating, its *own surface* (unlike the glass) was constrained

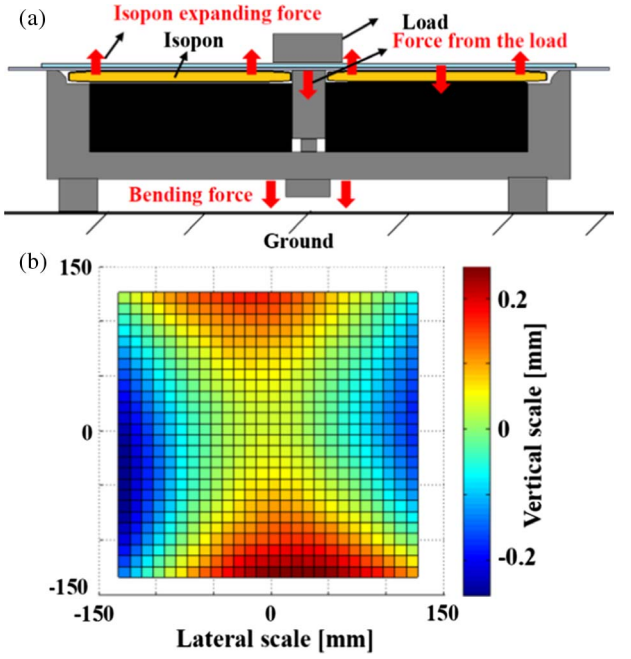

Fig. 6. (a) Method of creating a saddle surface and (b) created PV ~470 μm saddle surface measured by CMM.

to be axially symmetric. The tool profile after a run was measured on an Extended Range Form Talysurf, as shown in Fig. 8(b). The tool was indeed nominally flat, with PV departures of ~10 μm for the 9 μm abrasive and ~20 μm for the 20 μm abrasive. This is as expected, as the part was a saddle, and the tool surface takes up the rotationally averaged contour, which is essentially flat. There are second-order effects on precise tool profiles, such as increasing surface speed towards the periphery of a rotating tool and slurry migration effects when injecting on-axis.

2. Removal Depth

Figure 9 gives an example of the removal topography resulting from the surface before and after the grolishing process, as measured by the CMM.

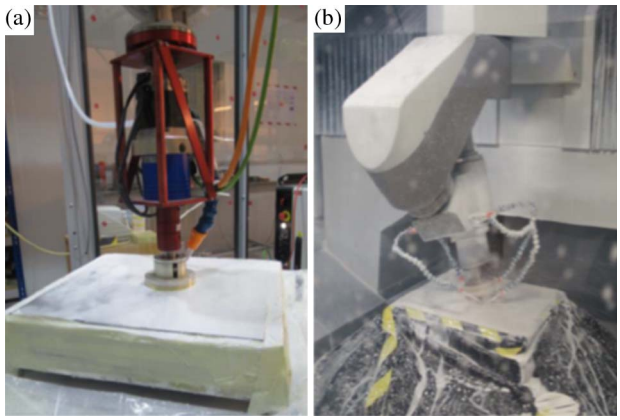

Fig. 7. (a) Robotic grolishing process and (b) IRP1200 polishing process.

Table 1. Variables for Grolishing Saddle Surfaces to Investigate on Set of MSFs

Variables		
Aqueous suspension of either 9 μm or 20 μm Al_2O_3 abrasives		
Controlled variables		
10 mm track space	600 rpm spindle speed	100 mm dia. tool
4500 mm/min tool feed	Slurry density = 1:6 (measured by weight)	Raster tool path (X)

Table 2. Controlled Variables for the Post-Polishing Process for Sample Measurement

1 mm track space	Slurry density = 1.03	R80 bonnet tool
800 mm/min tool feed	1000 rpm spindle speed	Raster tool path (Y)
1 mm point spacing	Cerium oxide abrasive	0.7 mm tool offset

3. MSF Measurements

From the experiments, it was found that the MSF signature from tool conditioning was removed by the subsequent grolishing process (Fig. 3), using the same parameters as in Table 1, but rastering in the orthogonal direction. Figure 10 shows that interferometry of the surface post polished on the IRP1200 machine was possible, over sub-areas of 60 mm diameter.

MSFs in the raw data were swamped by low-order aberrations. Thirty samples were measured using a 4D Technologies interferometer (model 6000) and analyzed using the 4Sight analysis software. Our results demonstrated that, in the 120 Zernike terms considered overall, the first 35 terms were associated with low-order aberrations. These were removed from

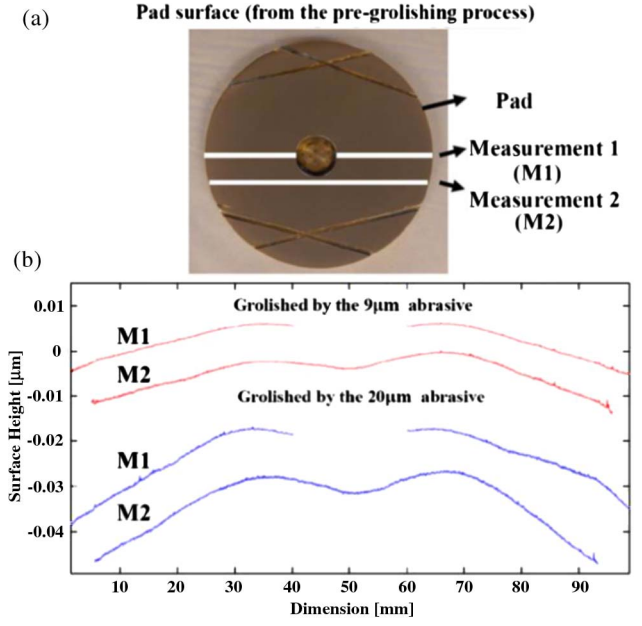

Fig. 8. Pad surface from the pre-grolishing process: (a) measurement directions of the pad surface and (b) pad surface profile.

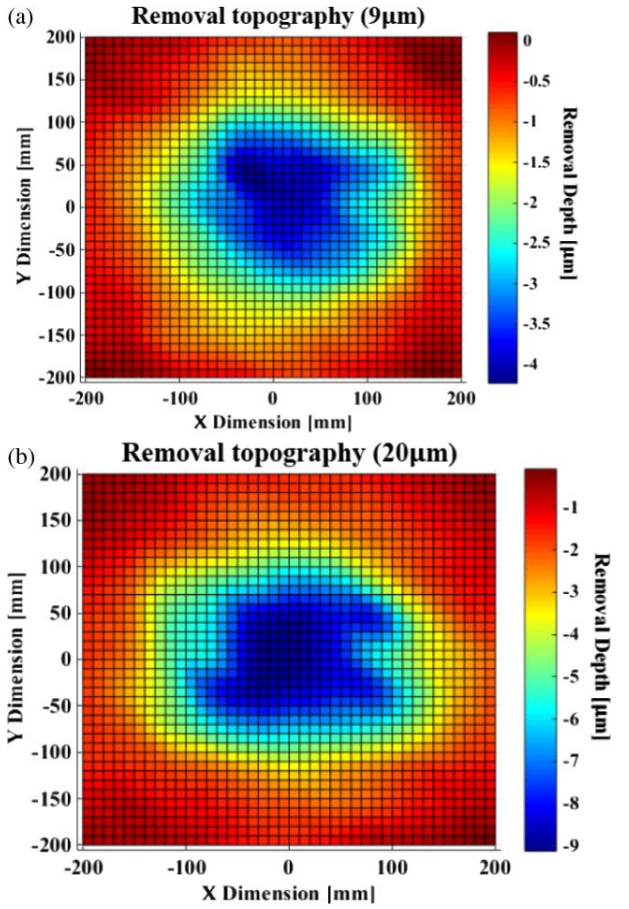

Fig. 9. Removal topography from the (a) 9 μm abrasive and (b) 20 μm abrasive grolishing process.

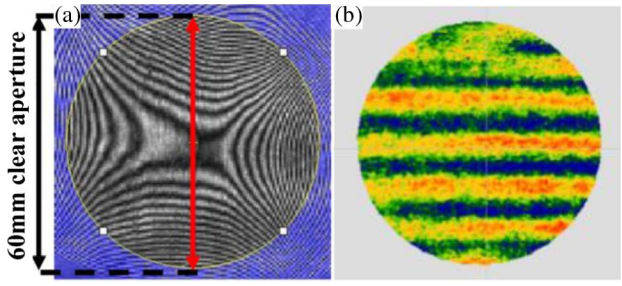

Fig. 10. (a) 60 mm measured area in 180 mm field of interferometer and (b) MSF results after removing 35 Zernike terms.

the data before determining MSF amplitudes. More data can be found in [6].

4. RESULTS AND DISCUSSION

To be meaningful, MSF measurements need to be placed on a common basis. After all, MSFs can be reduced to arbitrarily low levels simply by reducing the depth of material removal to near zero! Therefore, we have scaled measured MSF RMS values according to measured removal depth. The grolishing results are shown in Fig. 11(a). With the 20 μm abrasive, there is evidence of a significant flattening of the curve for low misfits, which we attribute to the particles filling the misfit voids. With the 9 μm abrasive, this is less clear, but such an effect is not inconsistent with the noise in the data. For this reason, the 9 μm experiment was repeated using two different track spacings: 5 mm and 10 mm, respectively. Note that all other parameters were kept the same; the run with 5 mm tracks took twice as long, and the resulting removal depth was doubled.

Results are shown in Fig. 11(b) and are interpreted as follows. For low and medium values of tool misfit with the asphere, the MSF content is dominated by the overlapping track-spacing effect, where increased track spacing leads to additional ripple on the surface. At high misfits, the MSF content is dominated by the misfit effect itself.

Returning to the prototype E-ELT segment fabrication at OpTIC, early in polishing the first segment (designated S1, centered 18.470 m from the axis of the parent asphere), attempts were made to use a 150 mm diameter rotating pitch

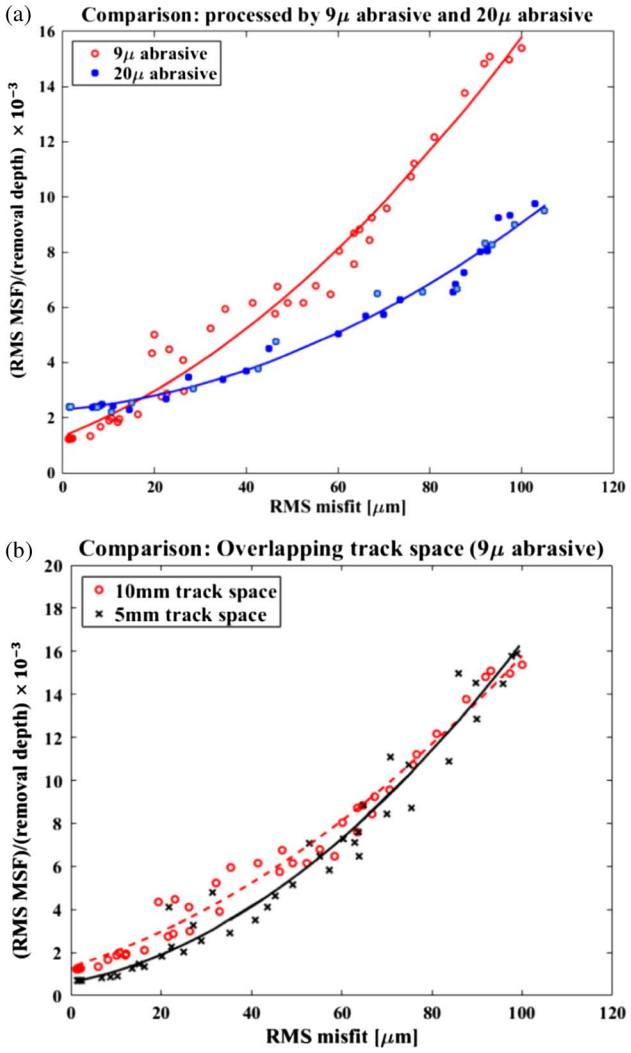

Fig. 11. Comparison: (a) processed by the 9 μm and 20 μm abrasives, respectively, and (b) overlapping track space by the 5 mm and 10 mm, respectively.

smoothing tool. This introduced MSFs and was replaced for all subsequent work by a similar 100 mm diameter tool, which proved satisfactory. For the telescope primary ROC of 84 m and conic constant −0.993295 [18,19], the dominant rotational component of the aspheric misfit with these tools was 1.50 μm and 0.67 μm PV, respectively. This may be compared with the quoted particle size of 1–2 μm for the Cerox 1663 cerium oxide slurry used. This is consistent with the abrasive slurry effectively cushioning the reduced aspheric misfit with the 100 mm tool, but not the increased misfit with the larger tool. This supports our belief that the principle is general.

5. CONCLUSION AND FUTURE WORK

In this paper, we have re-explored hard-tool smoothing of aspheres, which is usually avoided due to tool-misfit-induced MSFs. Using a novel glass-bending rig, both to create a variable complex surface form and to withstand process forces, we have quantified the relationship among tool misfit, abrasive grit size, and MSFs created on the surface. Results show that there is an advantageous "window," where the grit size is greater than the aspheric misfit over the tool size. In this case, the abrasive particles appear to cushion the gaps between tool and part, mitigating MSF creation. This appears to be fundamental, and should be scalable to more severe aspheres or freeforms.

In summary, it appears that hard-tool smoothing should be useable on aspheres, according to the following criteria, for any loose-abrasive step in the process chain:

The tool diameter should be chosen so that the tool misfit, anywhere on the surface of the part, is smaller than the abrasive particle size.

The maximum allowable tool diameter may, in some cases, be larger for a non-rotating tool, compared with a rotating tool. This will depend on the topography of the part, in particular, whether there is a strong cylindrical signature that favors non-rotating tools.

The work reported is particularly significant for edge control, given that a hard-tool smoothing step was an essential part of meeting the challenging edge-misfigure specification for the prototype E-ELT segments. Moreover, local edge figuring has wider potential for other applications, including other segmented systems, image and pupil slicers, and undersized mirrors in IR systems to minimize thermal background.

Our approach reported in this paper merits further investigation by ourselves and others. First, the quantitative reproducibility of the bending rig itself should be assessed for different bending regimes. Note that in the work reported, this was of secondary importance, as we have simply sought the relationship among particle size, misfit, and MSFs produced. In this case, the location on the surface at which a specific misfit appears is not of any particular importance. Nevertheless, an improved understanding of rig performance, including compliance of the silicone layer, would aid in establishing future experiments. Then, MSFs should be characterized for a wider family of abrasive sizes and tool misfits to establish a better sampling of the parameters space, and hopefully confirm the relationships that this preliminary study has discovered. This work should then be extended to considering the effects of changes in particle size as abrasives wear in use, which impacts both uniformity of constant-removal processes and convergence of corrective processes. Finally, the same experiments should be conducted using bound abrasives, representing a completely different removal modality, where grits are neither mobile nor able to rotate.

Funding. National Science Foundation (NSF) (1263236, 0968895, 1102301); The 863 Program (2013AA014402); Science and Technology Facilities Council (STFC) (ST/L001950/2, ST/L001985/2); China Scholarship Council (CSC).

Acknowledgment. Part of the work was supported by two linked UK-STFC grants under its IPS scheme. H. Y. Wu acknowledges financial support for his UCL PhD from the MOE Technologies Incubation Scholarship from the Ministry of Education, Taiwan. Peng Zhang is acknowledged for his work developing the Swinging Part Profilometer and making it available to this project. Wang Zhang and Chunlian Lu acknowledge their financial support from CSC. We also thank Dr. Christina Reynolds for her work developing the robot control software within the Zeeko software environment. We also thank the OpTIC center, St Asaph, for hosting the work and making available test equipment, including the CMM and sample preparation equipment.

REFERENCES

1. X. Tonnellier, P. Morantz, P. Shore, and P. Comley, "Precision grinding for rapid fabrication of segments for extremely large telescopes using the Cranfield BoX," Proc. SPIE **7739**, 773905 (2010).
2. H. Li, D. Walker, G. Yu, and W. Zhang, "Modeling and validation of polishing tool influence functions for manufacturing segments for an extremely large telescope," Appl. Opt. **52**, 5781–5787 (2013).
3. H. Li, G. Yu, D. Walker, and R. Evans, "Modelling and measurement of polishing tool influence functions for edge control," J. Eur. Opt. Soc. **6**, 110481 (2011).
4. S. C. West, H. M. Martin, R. H. Nagel, R. S. Young, W. B. Davison, T. J. Trebisky, S. T. DeRigne, and B. B. Hille, "Practical design and performance of the stressed-lap polishing tool," Appl. Opt. **33**, 8094–8100 (1994).
5. D. W. Kim and J. H. Burge, "Rigid conformal polishing tool using non-linear visco-elastic effect," Opt. Express **18**, 2242–2257 (2010).
6. D. D. Walker, D. Brooks, A. King, R. Freeman, R. Morton, G. McCavana, and S.-W. Kim, "The precessions tooling for polishing and figuring flat, spherical and aspheric surfaces," Opt. Express **11**, 958–964 (2003).
7. D. D. Walker, A. T. H. Beaucamp, D. Brooks, V. Doubrovski, M. D. Cassie, C. Dunn, R. R. Freeman, A. King, M. Libert, G. McCavana, R. Morton, D. Riley, and J. Simms, "Recent developments of precessions polishing for larger components and free-form surfaces," Proc. SPIE **5523**, 281–289 (2004).
8. D. Walker, A. Beaucamp, C. Dunn, R. Freeman, A. Marek, G. McCavana, R. Morton, and D. Riley, "First results on freeform polishing using the precessions process," in "*American Society for Precision Engineering (ASPE) Winter Topical Meeting on Free-Form Optics: Design, Fabrication, Metrology, Assembly*," CD-ROM (2004).
9. D. D. Walker, R. Freeman, R. Morton, G. McCavana, and A. Beaucamp, "Use of the 'Precessions' process for prepolishing and correcting 2D & 2½D form," Opt. Express **14**, 11787–11795 (2006).
10. D. Walker, C. Atkins, I. Baker, R. Evans, S. Hamidi, P. Harris, H. Li, W. Messelink, J. Mitchell, M. Parry-Jones, P. Rees, and G. Yu, "Technologies for producing segments for extremely large telescopes," Proc. SPIE **8126**, 4–9 (2011).
11. C. Gray, I. Baker, G. Davies, R. Evans, N. Field, T. Fox-Leonard, W. Messelink, J. Mitchell, P. Rees, S. Waine, D. D. Walker, and G. Yu,

"Fast manufacturing of E-ELT mirror segments using CNC polishing," Proc. SPIE **8838**, 88380K (2013).
12. H.-Y. Wu, G. Yu, D. Walker, X. Zheng, H. Li, C. Dunn, and C. Gray, "Optimisation of grolishing freeform surfaces with rigid and semi-rigid tools," Proc. SPIE **9912**, 99123Q (2016).
13. D. Walker, C. Dunn, G. Yu, M. Bibby, X. Zheng, H. Y. Wu, H. Li, and C. Lu, "The role of robotics in computer controlled polishing of large and small optics," Proc. SPIE **9575**, 95750B (2015).
14. D. Walker, G. Davies, T. Fox-Leonard, C. Gray, J. Mitchell, P. Rees, H. Y. Wu, A. Volkov, and G. Y. Yu, "Advanced abrasive processes for manufacturing prototype mirror segments for the world's largest telescope," Adv. Mater. Res. **1017**, 532–538 (2014).
15. G. Yu, D. Walker, and H. Li, "Implementing a grolishing process in Zeeko IRP machines," Appl. Opt. **51**, 6637–6640 (2012).
16. P. Zhang, J. Li, D. Walker, and G. Yu, "Development of swinging part profilometer for optics," Proc. SPIE **10151**, 101510B (2016).
17. H.-Y. Wu, "Statistical approach to control output surfaces from the robotic grolishing process."
18. P. Comley, P. Morantz, P. Shore, and X. Tonnellier, "Grinding metre scale mirror segments for the E-ELT ground based telescope," CIRP Ann.–Manuf. Technol. **60**, 379–382 (2011).
19. S. J. Thompson, R. Lang, P. Rees, and G. W. Roberts, "Reconstruction of a conic-section surface from autocollimator-based deflectometric profilometry," Appl. Opt. **55**, 2827–2836 (2016).